Nanostructure of supported lipid bilayers in water

Bert Nickel[a)]
Department für Physik and CeNS Geschwister-Scholl-Platz 1, Ludwig-Maximilians-Universität, D-80539 München, Germany

(Received 4 September 2008; accepted 3 October 2008; published 23 December 2008)

Biologically functional supported lipid bilayers (SLBs) used in the rising field of nanobiotechnology require fine tuning of the SLB interface with the substrate, e.g., a sensor surface. Depending on the application, membrane functionality implies a homogeneous and dense bilayer and a certain degree of diffusivity in order to allow for a rearrangement in response to, e.g., protein binding. Here, progress in the preparation, characterization, and application of SLBs obtained in the past three to five years are highlighted. Synchrotron techniques, which allow to reveal structural features within the membrane on a length scale of ~0.5 nm are discussed in more detail, as well as the relation of structural features to dynamical membrane properties obtained by complementary optical techniques. © *2008 American Vacuum Society.* [DOI: 10.1116/1.3007998]

I. INTRODUCTION

Membranes interface the inside and outside of a living cell. A cell membrane represents a highly asymmetric assembly of amphiphilic molecules including lipids, cholesterol, and proteins arranged in a sheet, which exhibits a lipid bilayer as its main structural motive.[1] Membrane function includes regulation of what comes into and what goes out of a cell, cell identification, and signal transduction.[2] About one-third of the human protein coding genes encode membrane proteins.[3] A comparable fraction of drugs targets membranes and membrane proteins. Understanding membrane function can be considered as a crucial step in developing new therapies in a rational way. Many aspects of membrane function are still under debate, in particular, the importance of lipid phase separation for the regulation of membrane function.[4] This is because the temporal and lateral arrangements of membrane constituents in a living cell membrane are not easy to access experimentally.

Micelles and vesicles, lipid monolayers at the air-water interface, and supported lipid bilayers (SLBs) all represent versatile model systems to study certain aspects of lipid membranes. Since vesicles and micelles represent the way lipids traffic in a living cell,[2] they are important model systems for drug or gene delivery. On the other hand, lipid monolayers adsorbed at the air-water interface can be manipulated using Langmuir techniques, allowing to study, in particular, packing aspects of lipids. SLBs, i.e., lipid membranes spread on a flat surface, have evolved more recently; they will be in the focus of this report.

A. SLBs and their applications in biosensing

The discovery how to prepare SLBs on glass slides[5] allowed researchers to employ established surface physics techniques to membranes *in vitro* with unprecedented accuracy. The techniques applicable to SLBs include surface plasmon resonance, quartz microbalance, atomic force microscopy, and x-ray and neutron reflectometries, as well as modern microscopy methods and electrical impedance measurements.

In the course of these experiments, the need for fine-tuned interlayers between the supporting substrate and the membrane was recognized. At the same time, application of optimized SLBs was envisioned for biomimetic surfaces which, for example, act as a template for an enzymatic reaction on a membrane surface.[6]

During the past years we have witnessed the emergence of nanotechnology, with a rapid development of key technologies such as microfluidics, chemically structured surfaces, and new transducer systems. SLBs represent an elegant way to add biofunctionality to such devices. The combination of SLBs with surface based electronical, mechanical, or optical transducers is therefore a rapidly developing field. Most of the sensoric applications for SLBs aim at quantifying binding of target molecules or, in general, the surface fraction occupied by an adsorbate.[7,8]

One early example of a biofunctionalized mechanical transducer is a SLB coated quartz microbalance crystal,[9] such a setup can be used to determine membrane associated protein binding to SLBs as a function of *p*H and ionic concentrations.[10] More recent developments in this direction include SLB coated microcantilevers, which bend upon protein absorption.[7] Examples for label-free optical transducers include waveguides for dual polarization interferometry[11] and nanostructured metal films for localized surface plasmon resonance.[8] In these experiments, evanescent light fields probe changes in the index of refraction at the membrane interface due to, e.g., protein absorption. Examples for electrical transducers include SLB coated field effect transistors (FETs) such as carbon nanotubes or silicon on insulator (SOI) devices.[12] Here, charges associated with protein absorption to SLBs couple into the FET and modify the working point.

[a)]Tel.: +49 (0)89 2180 1460; electronic mail: nickel@lmu.de

II. STRUCTURAL AND DYNAMICAL PROPERTIES OF SLBS

If supported membranes are to be used as well defined templates to study fundamental aspects of membrane protein interaction, experimental techniques are needed which can yield structural and dynamical information on the molecular level. Label-free optical methods usually rely on the variation of the index of refraction n with membrane configuration. In most cases, the spatial resolution of optical probes is inherently limited by the wavelength of light. Variations of the index of refraction on a nanometer scale are therefore beyond reach. Synchrotron x-ray[13–15] and neutron[16–18] experiments using angstrom wavelengths do not suffer this limitation. In the following, we will highlight how synchrotron reflectometry experiments resolve structural details of SLBs. Naturally, this review is biased toward our own experiments, however, we will try to set this work in a larger framework of synchrotron experiments dedicated to SLBs.

A. X-ray reflectometry

X-ray reflectometry is an experimental technique to probe electron density depth profiles $\rho(z)$. A monochromatic x-ray beam is reflected from the interface of a stratified media, e.g., a SLB fully immersed in water. The intensity of the reflected beam $I(\alpha)$ is recorded as a function of the angle α of the incident x-ray beam with the sample horizon. The reflected intensity $I(\alpha)$ is the outcome of multiple reflection and transmission processes due to variations in the index of refraction profile $n(z)$. $n(z)$ is related to the electron density depth profile $\rho(z)$ via

$$n(z) = 1 - \delta(z) + i\beta(z) \tag{1}$$

and

$$\delta(z) = \rho(z)\frac{\lambda^2 r_e}{2\pi}. \tag{2}$$

Here, λ is the x-ray wavelength and r_e is the classical electron radius. (This implies that the measurement is nonresonant and α is so small that the atomic form factors $f(q_z)$ can be approximated by $f(q_z)=Z$; Z is the number of electrons. Resonant scattering effects and the angular dependence of f are usually taken into account for numerical analysis. $\beta = \lambda\mu/(4\pi)$; μ is the absorption length.) The reflected intensity $I(\alpha)$ is commonly reported as a function of the momentum transfer $I(q_z)$. Here,

$$q_z = \frac{4\pi}{\lambda}\sin(\alpha). \tag{3}$$

The presence of the different layers gives rise to an interference pattern $I(q_z)$. In order to analyze this interference pattern, a model electron density profile $\tilde{\rho}(z)$ is constructed and a reflected intensity $\tilde{I}(q_z)$ is calculated[19] based on this profile. The model profile $\tilde{\rho}(z)$ is varied until the measured $I(q_z)$ and calculated $\tilde{I}(q)$ intensity coincide.

The smallest length scale Δz which can be resolved unambiguously by a reflectometry experiment is given by the largest momentum transfer $q_{\max}$ up to which the reflection signal $I(q_{\max})$ can be separated from the background. State of the art synchrotron experiments typically reach $q_{\max} \approx 0.5–0.7$ Å^{-1}, equivalent to a resolution of

$$\Delta z \approx \pi/q_{\max} \tag{4}$$

or $\Delta z \approx 6–4$ Å. The experimentally accessible profile $\rho(z)$ can be figured as a convolution of a theoretical profile by a Gaussian of width Δz representing the resolution of the experiment performed.

Let us estimate the theoretical electron densities $\rho(z)$ associated with the chemical groups of a phospholipid in a bilayer structure and the effective layer thicknesses d. As an example, let us consider liquid crystalline phase DMPC. For the lipid headgroup, one has to account for the choline (chol), phosphate (P), glycerol and carbonyl (gly) groups. For the chain part, one has to account for the alkane chain (–CH2–) and the methyl (–CH3) termini, cf. sketch in Fig. 1. To estimate the electron densities, the number of electrons associated with each group are divided by the molecular volume obtained from molecular dynamics of DMPC at 30 °C, i.e., in the liquid crystalline phase.[20] To estimate the effective layer thickness d, the volume of the group is divided by the

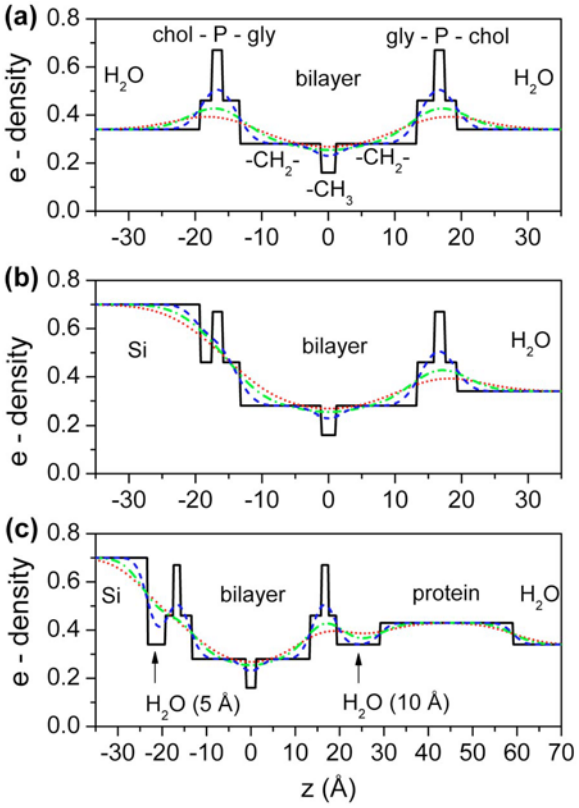

FIG. 1. *Estimate of electron density profiles.* The SLB electron density profile $\rho(z)$ estimated from molecular volume is shown as a black line. After convolution with a resolution function of 2 Å (dashed curve), 4 Å (dashed-dotted curve), and 6 Å (dotted curve), some of the submolecular details are smeared out. (a) Free floating bilayer, i.e., no substrate present. (b) SLB placed in direct contact with a Si surface. (c) SLB separated by a 0.5 nm water layer from a Si surface. The SLB is covered by a protein layer separated by a 1 nm water layer.

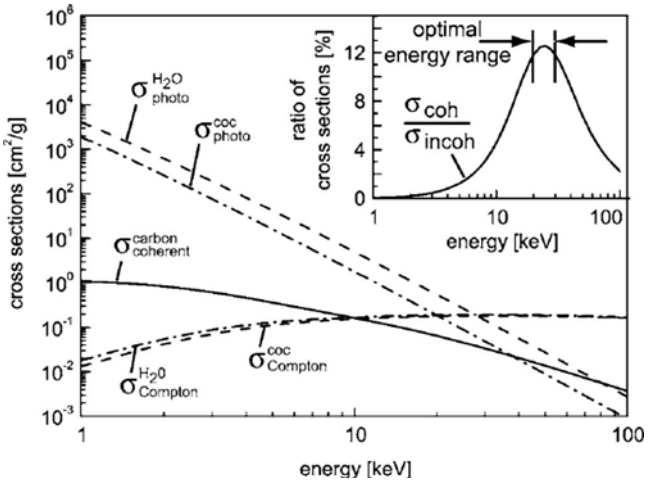

FIG. 2. *Simulation*. Energy dependence of the coherent and incoherent scattering cross section. Inset: optimal signal to noise ratio is observed for energies around 20 keV (Ref. 22).

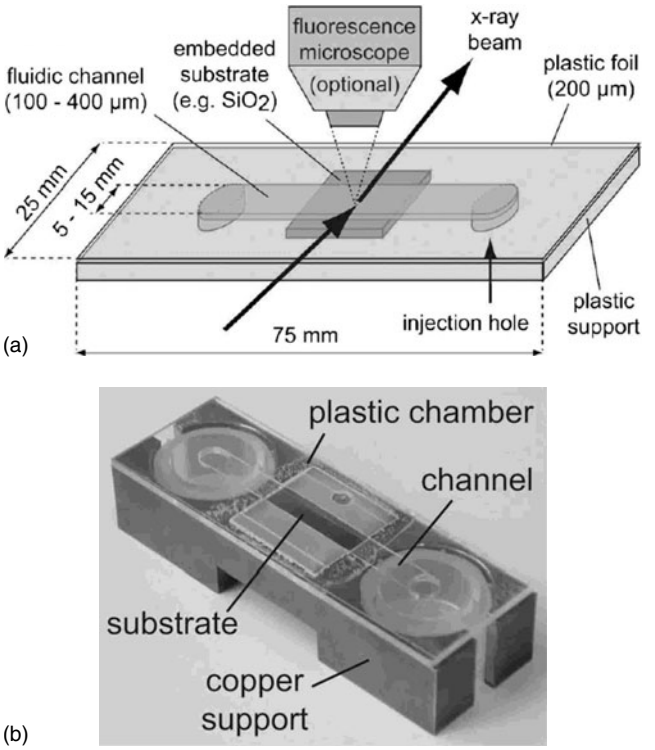

FIG. 3. *Sample cell*. Schematic (a) and photograph (b) of the microfluidic setup for membrane preparation and characterization by fluorescence microscopy and x rays (Ref. 22).

average area (A) per lipid. For DMPC, an angled profile $\rho(z)$ is obtained this way shown in Fig. 1(a) as black curve. Note that the electron density of the headgroup (0.46 $e^-/\text{Å}^3$ for choline and glycerol and 0.67 $e^-/\text{Å}^3$ for phosphate) is notably above the density of water (0.34 $e^-/\text{Å}^3$), while the alkane chain part is below (0.28 $e^-/\text{Å}^3$), and even lower for the methyl terminus (0.16 $e^-/\text{Å}^3$). The idealized profile of a free floating DMPC bilayer is convoluted by a 2 Å (dashed curve), 4 Å (dashed-dotted curve), and 6 Å (dotted curve) resolution function shown in Fig. 1(a). The 2 Å convolution reduces the contrast with water already considerably. Moreover, if the DMPC bilayer is placed in direct contact with a Si wafer [Fig. 1(b)], the headgroup density of the lipid facing the wafer crosses over monotonically to the Si density, making a localization of the headgroup difficult. If the SLB is separated from the Si interface by a 0.5 nm water gap [Fig. 1(c)], the 2 Å resolution measurement clearly resolves this water layer, while the 4 and 6 Å measurements, which are closer to the experimental situation, do not. Finally we note that a typical protein electron density is 0.44 ± 0.01 $e^-/\text{Å}^3$, [cf. Fig. 1(c)], thus high coverage protein layers should also be accessible in a reflectometry experiment.

B. Design of the x-ray experiment

For the study of SLBs, absorption of the x-ray beam while passing the water should be minimized and at the same time the coherent signal should be maximized. For soft materials such as organic molecules and water, the ratio of coherent and incoherent x-ray scattering cross sections exhibits a broad maximum around 18–20 keV (cf. inset in Fig. 2). This range represents the optimal choice for the x-ray energy in view of signal to noise ratio. Operating a synchrotron beamline at 20 keV imposes some constraints on the optical components. At second generation synchrotron sources such as HASYLAB, beamline D4 operates efficiently at 20 keV, while at third generation synchrotron sources such as ESRF and APS, much more instruments meet these constrains. At 20 keV, the attenuation length in water is $\mu = 14$ mm, which also represents the optimum sample size. In comparison, at 17.4 keV (Mo $K\alpha$), shorter samples should be used ($\mu = 10$ mm).

Practical aspects such as preparation and handling of the sample for reflectometry experiments have to be addressed properly. Also, a reliable quality control of the sample is needed prior to the x-ray or neutron experiment. In response to these demands, an experimental setup based on a microfluidic system made from a cyclic olefin polymer (COC), a thermoplastic polymeric material which is highly transparent for light[21] and x rays of 20 keV, has been presented.[22] The COC based microfluidic chamber[23] is shown in Fig. 3. A piece of Si wafer is embedded into the COC fluidic chamber; the chamber can be modified by a milling cutter to allow for individual sample size. The setup allows for a preparation of the SLB on chip by standard pipet based procedures such as vesicle fusion.

The COC foil provides also optical access for a reflection fluorescence microscope (e.g., Zeiss Axiotech) equipped with a long distance (63×) objective with cover slip thickness correction. If about 1% of the lipids are labeled by a fluorescent dye, the membrane can be imaged as a homogeneous bright sheet (Fig. 4). Inhomogeneities on a micron scale, e.g., uncovered regions or aggregates can be readily identified by inspection of the fluorescent intensity. The reduction in such inhomogeneity is a valuable criteria to optimize the preparation protocol of the SLB prior to subsequent scattering experiments. If a homogeneous membrane is

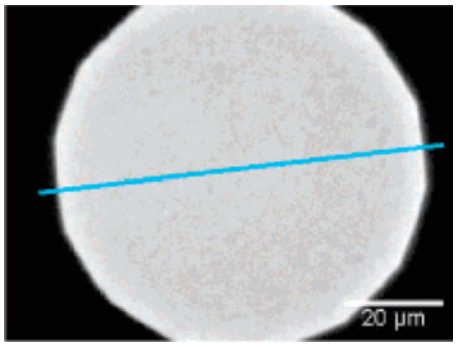

FIG. 4. *Fluorescence microscopy imaging.* SLBs are imaged using a small fraction of lipids with a fluorescent dye allowing to verify for membrane homogeneity and diffusivity (see text).

present (cf. Fig. 4), the second criteria are the diffusivity of the membrane components, a prerequisite for biological function in most cases. Continuous bleaching is a technique based on a fluorescence microscope to measure SLB diffusivity. In this technique, fluorescent dyes attached to a small fraction of lipids are photobleached during the continuous exposure. Consequently, the fluorescent image darkens with exposure time. However, at the rim of exposure, unbleached lipids diffuse. Thus, a fluorescence intensity profile builds up exhibiting a bright rim. Bleaching and diffusion rate can be determined from a time series of such intensity profiles.[24]

III. SLB ON SiO_2

A reflectivity curve for a 1,2-Dioleoyl-sn-Glycero-3-phosphocholine (DOPC)-SLB on SiO_2 is shown in Fig. 5.[22] The intensity exhibits a total reflection plateau for small momentum transfers, and an oscillating intensity decay over nine orders of magnitude covering a momentum transfer up to $q_{max}=0.5$ Å^{-1}. The intensity oscillations indicate the formation of a well defined layered structure. The q-range covered converts to a depth resolution of $\Delta z=6$ Å. The inset of Fig. 5 shows the electron density depth profile which models

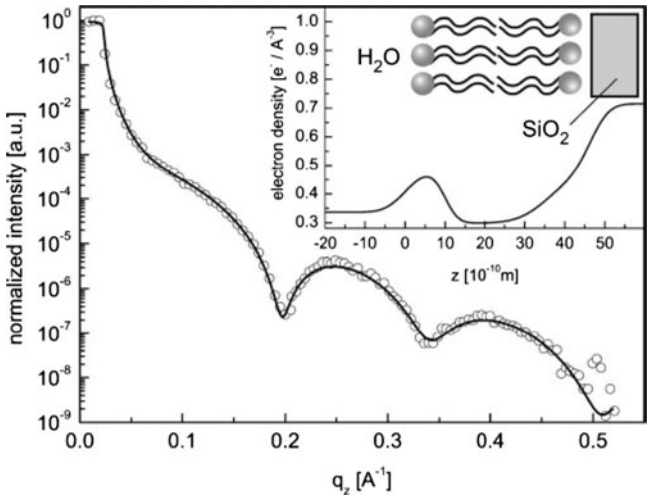

FIG. 5. *X-ray reflectometry data.* A DOPC membrane was spread on SiO_2. The solid curve is a fit to the data.

the observed experimental intensities correctly. Superimposed is the interpretation of the electron densities in terms of a bilayer model.[22]

This experiment addresses the question of how thick the water cushion between the lipid membrane and the adjacent SiO_2 substrate is. For the given example, the water layer cushion thickness is below the resolution limit, cf. also Figs. 1(b) and 1(c). Recent x-ray diffraction experiments agree in that for flat substrates, the water hydration layers on SiO_2 is 5 Å thick or less.[13]

IV. SLBS ON SOFT INTERLAYERS

If one wants to study the insertion of transmembrane proteins into membranes, the adjacent oxide surface will distort the protein configuration—in the worst case the protein denaturates. Soft interlayers acting as a cushion can reduce or, in the best case, avoid this problem.[6] In the following, we will show how x-ray reflectometry can be used to resolve the nanostructure of SLBs on technically relevant surfaces such as thermoplastic films and polyelectrolyte coatings. Tethered SLBs will be presented as an example for a chemically engineered surface. Furthermore, the potential of x-ray reflectometry for resolving molecular details of protein binding to membranes and the inner structure of multicomponent membranes is demonstrated.

A. SLB on a hydrophobic polymeric surface

COC is a polymeric material originally developed for DVD coatings and food packaging. It is thermoplastic, optically transparent, and well suited for cell culturing. Since COC is hydrophobic (contact angle ≈89°), the question emerges whether lipid coating of bilayer or monolayer structure can be achieved. To address this question, a 450 Å thin COC film was spin coated on a Si wafer piece, giving rise to rapid intensity oscillations in a reflectometry experiment, cf. data points (i) in Fig. 6(a). Once the chamber is filled with water, the rapid intensity oscillations associated with the COC film are weaker in amplitude [cf. data points (ii) in Fig. 6(a)]. A simulation of the experimental data verifies that this effect originates only from the reduced scattering contrast of COC with water compared to COC with air. The oscillation period is unchanged, indicating that the COC film does not swell in water.

Now a membrane is deposited by vesicle fusion, giving rise to a beating effect in the reflectivity curve [cf. data points (iii) in Fig. 6(a)]. This beating effect can be analyzed by a standard software packet (PARRAT32) which calculates the reflected intensity of stratified media. The result of such a simulation, which reproduces the experimental data quite well, is shown as line (ii) in Fig. 6(b). Adjacent to the COC film, the e-density first increases (lipid headgroup signature), then decreases (lipid chain signature), and then increases again, finally matching the density of water. These experiments suggest that a bilayer with a head-to-head distance of $d_{HH}=29$ Å forms on a COC support [cf. Figs. 7(b) and 7(c)]. In comparison, for a SiO_2 substrate, the head-to-head distance observed for this lipid is $d_{HH}=36$ Å [cf. Fig. 7(a)]. The

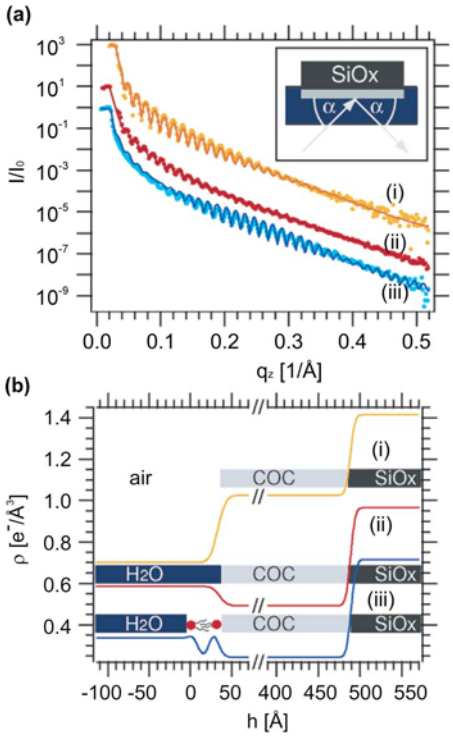

FIG. 6. *X-ray reflectometry data.* (a) Reflectivity curves of a uniform COC film on a Si wafer exposed to air [data points (i)] and in contact with water [data points (ii)] and with a DOPC layer prepared by vesicle fusion [data points (iii)]. Fits to the different curves are included as solid lines. The reflectivity curves are shifted vertically for clarity. The inset illustrates the setup used during reflectivity measurements. (b) Electron density profiles corresponding to the fits in (a). The profile for the COC layer on air is shown as line (i), the profile for the COC layer in water is displayed as line (ii), and the profile of a COC layer covered by a lipid membrane on top is depicted as line (iii). The profiles are shifted vertically for clarity. A cartoon illuminating the physical interpretation of the electron density profile is placed on top of each profile (Ref. 24).

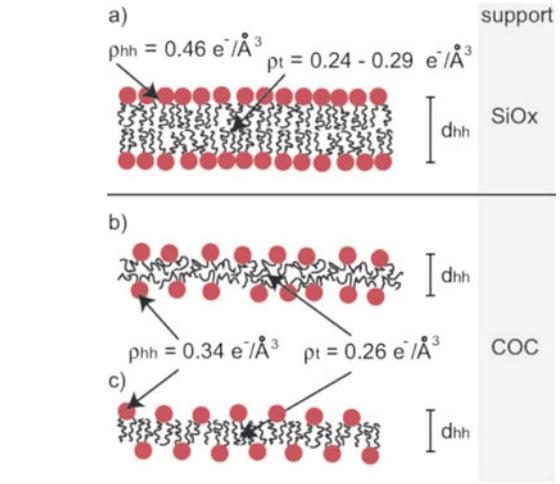

FIG. 7. *Bilayer configurations.* (a) Typical bilayer as found in DOPC membrane stacks or DOPC SLBs supported on SiO_x. (b) Thinned bilayer with coiled tails. (c) Thinned bilayer with interdigitated tails (Ref. 24).

reduced head-to-head distance on COC indicates a lipid configuration with either coiled tails [Fig. 7(b)] or interdigitated chains [Fig. 7(c)].

B. SLB on a charged polymeric surface

While COC is an interesting polymer due to its inertness, polyelectrolyte interlayers such as polyallylamine hydrochloride (PAH) are interesting polymeric materials due to their ability to form ultrathin but electrostatically stabilized layers.[25] In water, PAH physisorbs spontaneously to a SiO_2 surface, a negatively charged surface at neutral *p*H. Coating of SiO_2 surfaces by polyelectrolyte layers can be employed to reduce the *p*H response of FETs based on SOI technology.[26] Here, the polyelectrolyte coated surface is the top surface of the FET. For the modeling of the FET properties, precise knowledge of the polyelectrolyte layer thickness is needed to quantify the electronic coupling to the outside water phase and, in particular, FET response to the adsorption of charges molecules such as, e.g., DNA. Since the polyelectrolyte layer is strongly hydrated, it yields little or no scattering contrast to the adjacent water phase. However, the polyelectrolyte layer shows up in the depth profile if a suited

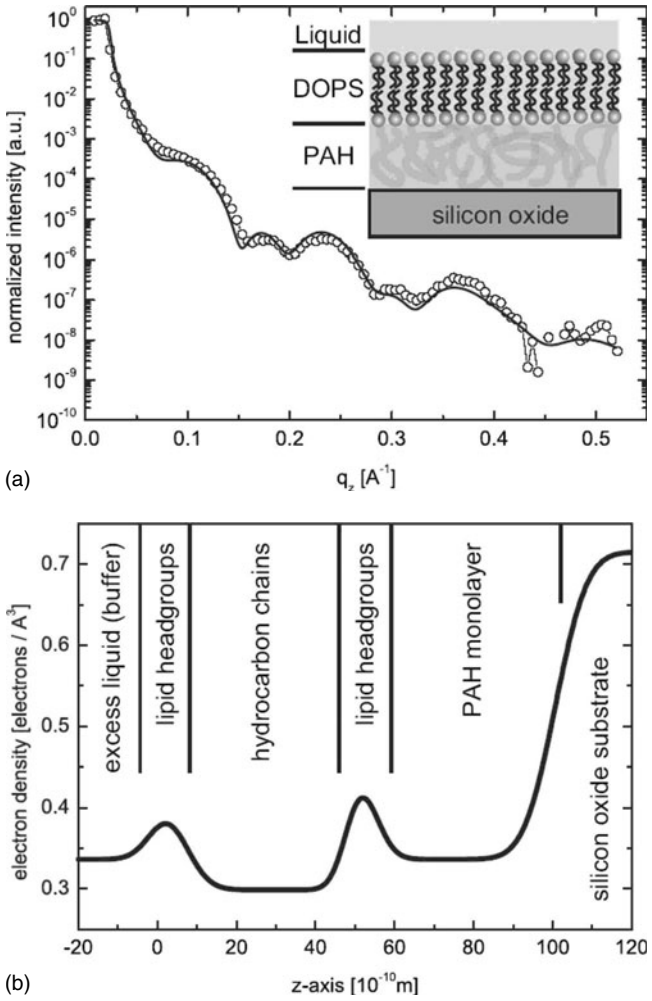

FIG. 8. *DOPS membrane on a PAH cushion.* (a) X-ray reflectivity of a DOPS membrane on a PAH cushion. The solid lines are fits to the data. (b) Electron density profile corresponding to the fit (Ref. 36).

lipid coating is absorbed on top of the PAH layer. The reflectivity data of such a layered structure are shown in Fig. 8(a). Modeling of the reflected intensities reveals a pronounced lipid bilayer signature [Fig. 8(b)] with a head-to-head distance of 49 ± 4 Å. This value indicates that an undistorted bilayer formed. The PAH interlayer can easily be determined from the density profile to be 40 ± 4 Å thickness.

C. SLBs on a lipo-polyethylene glycol self-assembled monolayer

A surface is usually considered inert or passive, if it does not participate in chemical reactions with its environment, or, more specifically, with water. If a surface is to be used in a biological environment, say, adjacent to tissue, the idea of inertness needs to be revised. A passive surface in a biological sense is a surface which does not distort the adjacent biological systems. A bare glass slide, for example, promotes adsorption and denaturation of water soluble proteins[27] and is therefore not considered as an inert surface in this sense.[28]

A neutral lipid membrane, i.e., a DOPC bilayer, is a rather inert surface in the sense that it will not promote the absorption of water soluble proteins. Bacteria such as E.coli ignore a SLB coated surface rather than attaching to it.[29] Some self-assembled monolayer (SAM) coatings can also prevent protein adsorption.[30,28] The most prominent example is polyethylene glycol (PEG).[31,32] This polymer suppresses the absorption of most proteins effectively and is considered as a potential coating for, e.g., implants or contact lenses. Here, we resumed the idea of grafting a lipo-PEG SAM to a SiO_2 surface, acting as a highly passive interlayer, which anchors a lipid bilayer, cf. Fig. 9(a).

The idea behind this architecture is that the topmost lipid bilayer can be easily biofunctionalized by spontaneous insertion or fusion of lipid anchored molecules, the very same mechanism which cells use to functionalize membranes.[2] The PEG interlayer below the membrane shields the biological components from the strongly absorbing SiO_2 substrate. The grafting of the lipo-PEG to the Si surface can be realized by silane chemistry.[33,34] This reaction is, however, very sensitive to tiny amount of water and cross-linking is difficult to avoid. Therefore, we have chosen a multistep reaction. The protocol starts with the formation of an octenyltrichlorosilane SAM. This SAM is then oxidized to the corresponding COOH termination, which is then further modified to *N*-hydroxysuccinimide. Finally, the amino-terminated, polyethylene glycol functionalized, 1,2-distearoyl-sn-glycero-3-phosphoethanolamine lipo-PEG2000 is fused to the SAM. To further densify the SAM, the last step was repeated with amino-terminated PEG of two different lengths, $n=17$ (PEG750) and $n=45$ (PEG2000). The chemistry scheme has been verified by x-ray photoelectron spectroscopy studies at various points of sample preparation.[35] Finally, a 1-Stearoyl,2-oleoyl-sn-Glycero-3-phosphocholine (SOPC) membrane has been spread using vesicle fusion. Bleaching experiments confirmed the presence of a fluid, homogeneous membrane.

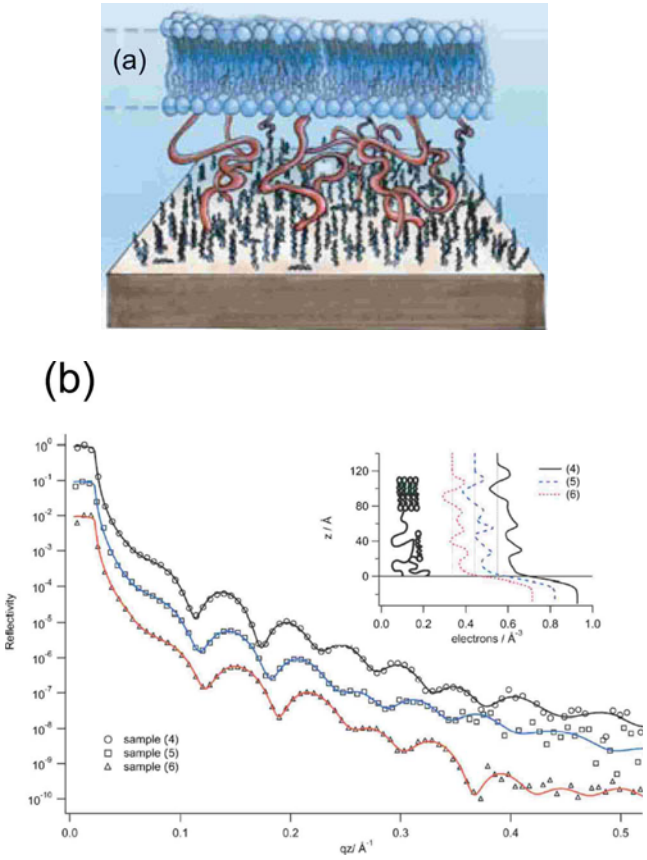

FIG. 9. *Tethered SLB.* (a) Schematic. A lipid bilayer tethered by a PEG interlayer to a SiO_2 surface (Ref. 35). (b) Reflectivity data and associated electron density profiles (inset).

X-ray reflectivity experiments of the SOPC membrane on top of the lipo-PEG interlayer are summarized in Fig. 9(b). Up to eight intensity oscillations are observed in a q-range up to 0.5 Å^{-1}, indicating the formation of a layered structure of $D \approx 8 \times 2\pi/0.5 = 100$ Å. Different colors in Fig. 9(b) encode different preparation schemes; the black curve labeled by (4) is the SLB spread on the lipo-PEG surface. The blue and red curves mark SLBs spread on lipo-PEG surfaces, which have been further densified by additional binding of PEG750 (5) and PEG2000 (6), respectively.

A detailed analysis [solid curves in Fig. 9(b)] reveals a 40 Å thick lipid bilayer, which is lifted from the SiO_2 interface by 70–80 Å, depending on the details of the preparation. This result is very promising, since it indicates that rather large transmembrane proteins could be inserted into the topmost bilayer without getting in contact with the SiO_2 substrate. A diffusion constant $D \sim 2.1$ $\mu m^2/s$ has been obtained for the elevated membrane from continuous bleaching experiments. This coincides with the value obtained for SOPC SLBs directly deposited on SiO_2.

V. CONCLUSIONS

In summary, we were able to deposit lipid bilayer on all soft interfaces explored. While a distorted, thinned out bilayer is observed for the hydrophobic support (COC),[24] the

charged matched PAH interlayer (positively charged interlayer and negatively charged DOPS lipid headgroup) rather increased the bilayer thickness,[36] presumably due to better packing induced by the electrostatic interaction at the interface. The elevated, lipo-PEG anchored bilayer thickness, in contrast, almost matches the value for free stacks.[35] Since the thickness of a bilayer has implications for the insertion of transmembrane proteins,[37] elevated membranes seem most suited for such application.

For the COC substrate, one might have expected the formation of a lipid monolayer structure with the hydrophobic chains pointing toward the substrate. Recently, a thermodynamic argument has been put forward suggesting that the bilayer midplane can be considered as a fluid-fluid interface.[38] Coexistence of ordered fluid with a disordered fluid is accompanied by an interfacial energy penalty of the order of $\sim 0.5\ \mathrm{kT/nm^2}$, enough to suppress what is called overhang in lipid vesicles.[38] Similarly, a fluid lipid monolayer on a moderately hydrophobic solid polymer substrate should also be unfavorable. Hybrid lipid membranes (i.e., a single lipid leaflet on a hydrophobic SAM) have been observed *per se* only for strongly hydrophobic SAM substrates with contact angles larger than 109° (Ref. 16) while COC exhibits a contact angle of $\sim 90°$.[24] It might well be that distorted bilayer formation on technically relevant polymer surfaces with moderate hydrophobicity are the rule, rather than the exception.

ACKNOWLEDGMENT

Financial support was provided by the BMBF (Nos. 03Ra6LMU and 03Ra7LMU), EU-Biodot, Elite Netzwerk Bayern, CeNS, and Nanosystems Initiative Munich (NIM). The x-ray experiments were performed at HASYLAB in Hamburg and at ESRF in Grenoble, with generous travel support. This review summarizes experimental results from Ph.D. students M. Hochrein, C. Reich, C. Daniel, and from postdoc visitor L. Andruzzi. The author gratefully acknowledges their contributions.

[1]S. J. Singer and G. L. Nicolson, Science **175**, 720 (1972).
[2]B. Alberts, *Molecular Biology of the Cell* (Garland Science, New York, 2002).
[3]W. L. Smith, R. M. Garavito, and S. Ferguson-Miller, J. Biol. Chem. **276**, 32393 (2001).
[4]K. Simons and E. Ikonen, Nature (London) **387**, 569 (1997).
[5]L. K. Tamm and H. M. McConnell, Biophys. J. **47**, 105 (1985).
[6]E. Sackmann, Science **271**, 43 (1996).
[7]Y. Zhang, S. P. Venkatachalan, H. Xu, X. Xu, P. Joshi, H. F. Ji, and M. Schulte, Biosens. Bioelectron. **19**, 1473 (2004).
[8]M. P. Jonsson, P. Jonsson, A. B. Dahlin, and F. Höök, Nano Lett. **7**, 3462 (2007).
[9]C. A. Keller and B. Kasemo, Biophys. J. **75**, 1397 (1998).
[10]K. Kastl, M. Ross, V. Gerke, and C. Steinem, Biochemistry **41**, 10087 (2002).
[11]T. Oikawa, H. Yamaguchi, T. Itoh, M. Kato, T. Ijuin, D. Yamazaki, S. Suetsugu, and T. Takenawa, Nat. Cell Biol. **6**, 420 (2004).
[12]M. G. Nikolaides, S. Rauschenbach, S. Luber, K. Buchholz, M. Tornow, G. Abstreiter, and A. R. Bausch, ChemPhysChem **4**, 1104 (2003).
[13]C. E. Miller, J. Majewski, T. Gog, and T. L. Kuhl, Phys. Rev. Lett. **94**, 238104 (2005).
[14]E. Novakova, K. Giewekemeyer, and T. Salditt, Phys. Rev. E **74**, 051911 (2006).
[15]C. E. Miller, J. Majewski, E. B. Watkins, D. J. Mulder, T. Gog, and T. L. Kuhl, Phys. Rev. Lett. **100**, 058103 (2008).
[16]C. W. Meuse, S. Krueger, C. F. Majkrzak, J. A. Dura, J. Fu, J. T. Connor, and A. L. Plant, Biophys. J. **74**, 1388 (1998).
[17]C. Delajon, T. Gutberlet, R. Steitz, H. Mohwald, and R. Krastev, Langmuir **21**, 8509 (2005).
[18]S. Lecuyer, G. Fragneto, and T. Charitat, Eur. Phys. J. E **21**, 153 (2006).
[19]L. G. Parratt, Phys. Rev. **95**, 359 (1954).
[20]J. B. Klauda, N. Kuerka, B. R. Brooks, R. W. Pastor, and J. F. Nagle, Biophys. J. **90**, 2796 (2006).
[21]T. Rohr, D. F. Ogletree, J. M. J. Svec, and F. Fréchet, Adv. Funct. Mater. **13**, 264 (2003).
[22]C. Reich, M. B. Hochrein, B. Krause, and B. Nickel, Rev. Sci. Instrum. **76**, 095103 (2005).
[23]ibidi Integrated Biodiagnostics.
[24]M. Hochrein, C. Reich, B. Krause, J. O. Rädler, and B. Nickel, Langmuir **22**, 538 (2006).
[25]R. v. Klitzing, Phys. Chem. Chem. Phys. **8**, 5012 (2006).
[26]P. A. Neff, A. Naji, C. Ecker, B. Nickel, R. Von Klitzing, and A. R. Bausch, Macromolecules **39**, 463 (2006).
[27]M. A. Polizzi, R. M. Plocinik, and G. J. Simpson, J. Am. Chem. Soc. **126**, 5001 (2004).
[28]E. Ostuni, R. G. Chapman, M. N. Liang, G. Meluleni, G. Pier, D. E. Ingber, and G. M. Whitesides, Langmuir **17**, 6336 (2001).
[29]T. Eichinger, Diploma thesis, Ludwig-Maximilians-Universitat, 2006.
[30]E. Ostuni, R. G. Chapman, R. E. Holmlin, S. Takayama, and G. M. Whitesides, Langmuir **17**, 5605 (2001).
[31]R. L. C. Wang, H. J. Kreuzer, and M. Grunze, J. Phys. Chem. B **101**, 9767 (1997).
[32]P. Harder, M. Grunze, R. Dahint, G. M. Whitesides, and P. E. Laibinis, J. Phys. Chem. B **102**, 426 (1998).
[33]S. R. Wasserman, Y. T. Tao, and G. M. Whitesides, Langmuir **5**, 1074 (1989).
[34]M. Calistri-Yeh, E. J. Kramer, R. Sharma, W. Zhao, M. H. Rafailovich, J. Sokolov, and J. D. Brock, Langmuir **12**, 2747 (1996).
[35]C. Daniel, K. E. Sohn, T. E. Mates, E. J. Kramer, J. O. Rädler, E. Sackmann, B. Nickel, and L. Andruzzi, BioInterphases **2**, 109 (2007).
[36]C. Reich, P. A. Neff, A. R. Bausch, J. O. Rädler, and B. Nickel, Phys. Status Solidi A **203**, 3463 (2006).
[37]F. Dumas, M. C. Lebrun, and J.-F. Tocanne, FEBS Lett. **458**, 271 (1999).
[38]M. D. Marcus, Biophys. J. **94**, L32 (2008).